SAND2019-8435J

Approaches to multi-scale analyses of mechanically and thermally driven migration of fluid inclusions in salt rocks

Hua Shao[1,#], Yifeng Wang[2], Olaf Kolditz[3,4] Thomas Nagel[3,5], Torben Brüning[1,4]

1. Federal Institute for Geosciences and Natural Resources (BGR), Hannover, Germany
2. Sandia National Laboratories (SNL), Albuquerque, USA
3. Helmholtz Centre for Environmental Research (UFZ), Leipzig, Germany
4. Technische Universität Dresden, Dresden, Germany
5. Technische Universität Bergakademie Freiberg, Freiberg, Germany

Corresponding author: shao@bgr.de

Abstract

Fluid inclusions are found within mineral crystals or along grain boundaries in many sedimentary rocks, notably in evaporite formations, and can migrate along a thermal or hydro-mechanical gradient. Shale and salt rocks have been considered potential host rocks for radioactive waste disposal, due to their low permeability. Previously stagnant inclusions may become mobilised by a perturbation of the in situ state by a geotechnical installation or the emplacement of heat-generating waste. The migration of fluid inclusions can thus have important impacts on the long-term performance of a geologic repository for high-level radioactive waste disposal. As a part of the international research project DECOVALEX-2019, two aspects of fluid inclusion migration in rock salt are currently investigated under different boundary conditions: a) altered hydro-mechanical conditions as a consequence of tunnel excavation or borehole drilling and b) coupled thermo-hydro-mechanical-chemical conditions during the heating period of the post-closure phase of a repository. To obtain a mechanistic understanding of underlying physical processes for fluid inclusion migration, a multi-scale modelling strategy has been developed. Hydraulic and time-dependent mechanical conditions due to the creep behaviour of rock salt for a microscale modelling are constrained by considering the macroscale stress evolution of an underground excavation. An analysis using a coupled two-phase flow and elasto-plastic model with a consideration of permeability variation indicates that a pathway dilation along the halite grain boundary may increase the permeability by two orders of magnitude. The calculated high flow velocity may explain the fast pressure build-up observed in the field. In addition, a mathematical model for the migration and morphological evolution of a single fluid inclusion under a thermal gradient has been formulated. A first-order analysis of the model leads to a simple mathematical expression that is able to explain the key observations of thermally driven inclusion migration in salt. Finally, numerical methods such as a phase field method for solving a moving boundary problem of fluid inclusion migration have also been explored.

Keywords: rock salt, fluid inclusion, coupled HM and THM processes, multi-scale modelling concepts, DECOVALEX

1 Introduction

Fluid inclusions containing a single phase (e.g., brine or methane) or multi-phases (e.g., hydrocarbons) can be found within mineral crystals (intra-crystalline) or along grain boundaries

Sandia National Laboratories is a multimission laboratory managed and operated by National Technology & Engineering Solutions of Sandia, LLC, a wholly owned subsidiary of Honeywell International Inc., for the U.S. Department of Energy's National Nuclear Security Administration under contract DE-NA0003525.

(inter-crystalline) in bedded and domed salt rocks (Anthony and Cline, 1971; Anthony and Cline, 1972; Roedder, 1984; Müller and Zschätsch, 1985; Müller, 1985; Hammer et al., 2013; Ghanbazadeh et al., 2015). They are formed under various pressure and temperature conditions during the formation's genesis. The size of the fluid inclusions ranges from several micrometres to millimetres, thus warranting a microscale study in understanding large-scale fluid flow and transport. These fluid inclusions are usually dispersed in a very low concentration. However, a significant quantity of local gas or liquid accumulations, up to hundreds of cubic meters, has been encountered in mines and can potentially lead to a catastrophic event (Minkley et al., 2018).

Such inclusions have been quantitatively studied in an exploration facility located in salt formation in Germany (Hammer et al., 2013; Thiemeyer et al., 2015; Paul et al., 2015). Since they are enclosed in mechanical equilibrium by the surrounding host rock, the initial fluid inclusions in an undisturbed rock are subjected to a lithostatic pressure, which is much higher than a corresponding hydrostatic pressure in the deep subsurface. Because of the low rock permeability and in many cases the absence of a connected pore space, the migration of such fluids under isotropic stress (confining pressure) conditions is almost impossible even under a high hydraulic gradient. The permeability of an undisturbed tight rock such as rock salt is much lower than 10^{-21} m² and often close to or below detection limits (Bräuer et al., 2011). Only diffusion processes may occur in those environments. Fluid release from grain boundaries will take place if the stress state changes sufficiently. In a construction and the operating phase of a geologic repository, stresses around the opening will be redistributed due to a drilling or an excavation, resulting in a deviatoric stress state altering the previously isotropic lithostatic state as present in salt formations. Consequently, the fluid pressure may exceed the minimum principal stress, leading to a possible formation of intragranular micro-cracks and an increase pore connectivity along intercrystalline grain boundaries, both of which can significantly increase the rock permeability. These phenomena are called dilatancy-controlled fluid migration (Xu et al., 2013).

With regard to the long-term performance of a potential geologic repository, undetected fluid inclusions may migrate in the presence of a thermal gradient. Experimental evidence (Roedder, 1970; Roedder, 1984) indicated that the inclusions in salt samples from the WIPP site might separate into a large liquid-rich part with trailing fins that moves toward a heating source and a small dumbbell-shaped gas-rich part that moves away from the heating sources. Similar observations were made by Anthony and Cline (1972) and Müller (1985). Based on a two-phase transport consideration and interface kinetics, a microscale model for bi-phasic inclusion migration was developed by Anthony and Cline (1972). Using this model, they reported that vapour-liquid droplets could migrate up to 6 m into the salt formation around a heat source within 2 years. On the other hand, the effects of fluid inclusions on creep have been reported (Thiemeyer et al., 2015). Mechanical creep behaviour changes in the presence of fluid inclusions (Urai et al. 2007; Knauth et al., 2018). Information on the effect of stress gradients can be found in Jenks (1979). Schlich (1986) investigated the mobilised aqueous and gaseous components in the fluid inclusions in the temperature field and the relevant transport mechanism. A simple numerical evaporation front model was used to simulate the movement of the two kinds of inclusions without coupling of mechanical processes.

It is important to characterize and quantify the distribution, amount and composition of fluid inclusions. Fluid composition offers useful information for regarding dissolution and precipitation processes. The migration rates under a range of thermal gradients yet need to be quantified as well as the evolution of the fluid inclusion pattern in terms of size and composition. The work presented below is aimed at enabling a quantification of mass transport into openings, which can constitute a water source for gas-forming corrosion processes, and away from openings, which can act as a radionuclide transport pathway. For the long-term performance assessment of a repository of radioactive high-level waste, the time scales of that transport need to be quantified.

Within the framework of the international collaborative project DECOVALEX (DEvelopment of COupled models and their VALidation against EXperiments), benchmark tests and exercises are designed for continuously improving simulation tools for various geotechnical applications, e.g. developing robust, predictive thermal-hydrologic-mechanical-chemical (THMC) modelling tools for a long-term performance assessment of deep geological repositories (Birkholzer et al., 2018). In the current phase DECOVALEX-2019, a task named FINITO (Fluid Inclusion and Movement in Tight Rock), focusing on fluid inclusions in rock salt, is jointly studied. The objective of this task is to obtain a better understanding of underlying physical processes of fluid inclusion migration and to develop appropriate numerical tools to explain laboratory and field observations.

In the present work, a multiscale modelling strategy is adopted. For both macroscale and microscale models, coupled hydraulic-mechanical (HM) processes for the construction phase of a geological repository and coupled thermal-hydraulic-mechanical (THM) processes for the post-closure phase are studied. The local stress field under hydraulic conditions around an opening after the excavation and during the heating phase is simulated using a macroscale model. Then, specific configurations will be analysed for the microscale modelling. At the microscale, the solid and fluid phases occupy different parts of the porous medium domain and interact at their common interface. The microscopic fields, which describe the properties of constituents, may be considered as continua within a single phase, while exhibiting discontinuities at the interfaces between phases. Often at such scales, fluid flow is described by the Stokes equations (Catalano et al., 2011). Due to very small Reynolds numbers in the flow through tight rocks, the Stokes equation can be simplified to a Darcy's law-based formulation.

Recently, pore-scale and microscale modelling of coupled processes in porous media has attracted significant attention (Blunt, 2001; Ferrari, 2014). Different methods, such as finite element methods (Glowinski et al., 2001) or Lattice-Boltzmann (Han et al., 2007) methods, have been introduced to analyse the coupled hydromechanical behaviour at the microstructure. However, these methods have their own limitations. Pinyol et al. (2012) follow the concept of incorporating the microstructural features in a constitutive model. The microstructure is quantified by the ratio of the microstructural void ratio (intra-aggregate space) and the total void ratio (Catalano et al., 2011). Microstructural void ratio can be determined if an intrusion-extrusion curve of MIP (Mercury Intrusion Porosimetry) are available. Pore network models are also widely used which are based on a simplified representation of porous media as a network of pores and throats (Ferrari, 2014).

In general, a microscale model requires a detailed understanding of the physical processes occurring at the pore scale and a detailed description of the morphology of the pore space (Al-Gharbi, 2004). Some ambiguity is always present, but the trick is to understand whether such ambiguity is important for the end-point of interest. For this, several technical methods have been developed in the fields of optical mineralogy and petrography, e.g. thin sectioning laboratory, CT (Computer Tomography) scanning, X-ray-based approaches, and SEM (Scanning Electron Microscopy) (Urai, et al., 1987; Schenk, et al., 2004; Thiemeyer et al., 2013). With the help of these methods, materials previously considered as ”homogeneous” may now be observed to exhibit a pronounced micro-structural inhomogeneity (Leben et al., 2003; Ölu et al., 2005). Different mineral compositions in a ”homogeneous” material possess different physical and chemical properties and their reactions can now be observed in a more direct manner at the microscopic level.

The present paper starts with a compilation of experimental and field observations concerning fluid inclusions in salt rock (section 2). Based on experimental evidence two cases are investigated in more detail: fluid movement due to a stress redistribution (section 3) and fluid migration due to thermal gradients (section 4). For both cases, both micro- and macroscale approaches are suggested and illustrated with simplified examples. This paper is not intended to be complete in addressing the issues related to fluid inclusion migration. Rather, it is focused on presenting some preliminary results and providing a perspective for future research (section 5).

2 Experimental and field observations of fluid inclusions and their movement

In an exploration facility located in rock salt in North Germany (Hammer et al., 2013; Paul et al., 2015) extensive microscopic studies on the sample structure using e.g. laser microscopy, computer tomography scans, electron backscatter diffraction (EBSD) have been conducted to characterize the morphology of pore space (Thiemeyer et al., 2013). These information can be used to construct numerical meshes for microscale simulations. The maximum porosity of a salt sample occupied by fluid inclusions was estimated to be 1.26%. Pores are particularly common along grain boundaries and healed microfractures. Using resin techniques, Thiemeyer et al. (2013) identified different shapes of grain boundaries at the pore scale decorated with a large number of fluid inclusions preserved as bubbles, stripes, branching networks, vermicular lines and fluid films (Figure 1). Different shapes of inclusions are the result of capillary forces in different geometric structures.

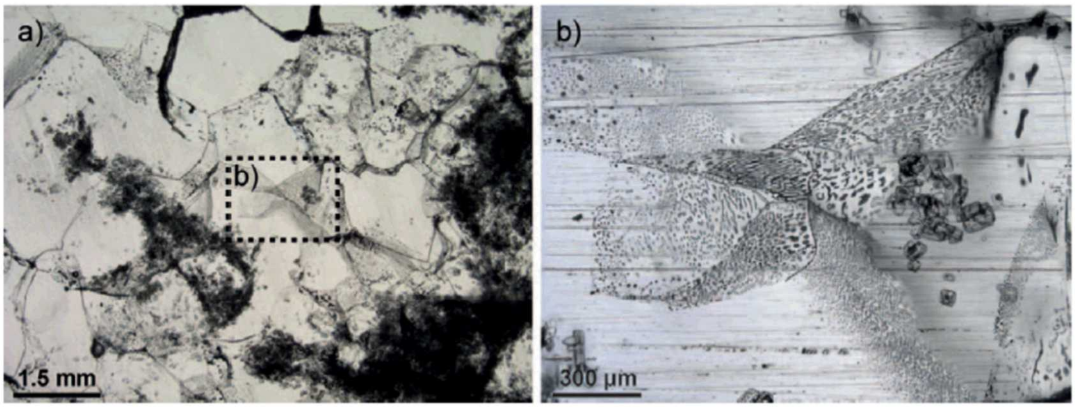

Figure 1: Halite grain boundaries decorated with fluid inclusions (Thiemeyer et al., 2013).

In addition, a long-term in situ investigation program (Paul et al., 2015) was conducted aiming to determine the volume of fluid inclusions and to study their potential connectivity among them. Twenty boreholes have been drilled and a special packer was installed in each borehole. The valve is opened if the interval pressure is higher than 2 MPa for reasons of mining safety. Up to several litres of influx originating from fluid inclusions have been collected from some boreholes. The packed-off intervals for the collection of fluid inclusions in the borehole are designed to lie outside of a so-called near-field damage zone of a larger excavation. A wide range of different amounts of fluid inclusions have been measured according to the geological investigation on the drilling core. The maximal measured hydrocarbon volume from an intensive borehole amounts to 16 litres of aqueous condensate and 4.6 m^3 gas within a period of 420 days. Based on the core sample scanning, the occurrence can be classified to:

a. Inclusions clearly visible under common artificial light,
b. Inclusions slightly visible only under ultraviolet light, and
c. No inclusions (referential boreholes).

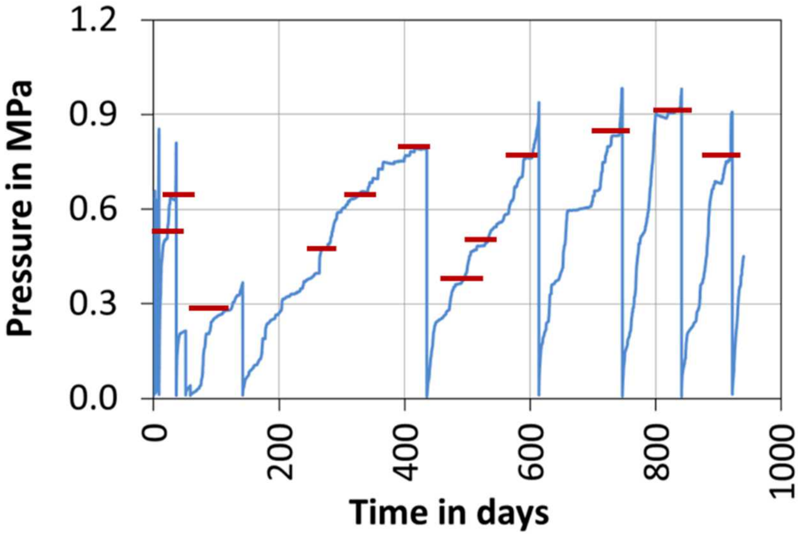

Figure 2: Stepwise increase in pressure indicate fluid release from localized individual fluid inclusions (Paul et al., 2015) (the red bars indicate the spontaneous steady state).

Figure 2 shows a typical pressure build-up in a borehole, which indicates fluid release from localized individual fluid inclusions. Such kind of pressure build-up is observed in the boreholes with a moderate inflow rate. Based on the information about the stepwise increase of the interval pressure, the inclusions are postulated to be unconnected with each other in the initial state. A pressure plateau (red bars in Figure 2) indicates a pressure equilibrium in the system before another inclusion with much higher initial pressure contributes to the fluid balance leading to a higher level of pressure. This process repeats until all inclusions in the influence area flow out. After a monitoring time of 940 days, the flow rate remains high. The continuous inflow with a relatively high increase rate can be explained by a possible generation of flow channelling between grain boundaries with high permeability.

Other experiments have been conducted on samples from rock salt to analyse the impacts of fluid inclusions on the safety of a repository. Information on the migration of liquid and liquid-gas droplets under thermal gradients, including shape changes, droplet disintegration and coalescence, and rate-determining factors are available from literature (Anthony et al., 1971; Anthony et al., 1972; Cline et al., 1977; Müller et al., 1985). An extensive literature review of experimental and theoretical studies of brine migration in salt can be found in Jenks (1979). They also derive an empirical expression for the maximum migration velocity in a temperature field and estimate its effects on high-level-waste (HLW) repository performance. In addition to temperature gradients the influence of stress ("pressure") gradients is discussed and found to result in "a small fractional increase" of solubility.

A considerable contribution to this field is the work by Roedder (1984), who summarised the status of the study of the types of fluids present in salt, their origin and evolution, and their significance for understanding geological processes. He performed small-scale laboratory measurements of the migration rates, using single crystals of salt. Blocks of salt about 1 cm cube and containing selected inclusions were prepared and the positions of the inclusions measured relative to scribed fiducial marks. The blocks were then heated to a specified temperature (Figure 3). Additionally, a temperature gradient of 1.5 K/cm was superimposed and maintained for 3-10 days. The migration rates for inclusions in different parts of a given sample were found to vary by a factor of 3. The three major controlling variables seem to include inclusion size, temperature and temperature gradient. However, theoretical considerations and some experimental studies (Anthony et al., 1972; Müller et al., 1985) suggest that the migration rate may also be related to the fluid composition, the presence of gas, its pressure, mechanical strain, dislocation abundance and nature, crystallographic direction, and radiation damage.

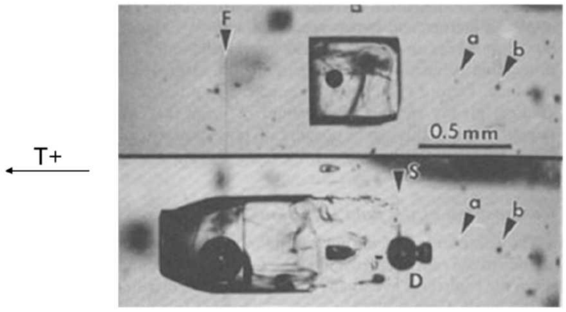

Figure 3: Experimental observation on fluid-migration after 156-hours run at 202°C ambient and 1.5 K/cm gradient (Roedder, 1984).

Taken together, these observations motivated the two cases for the task study in the current DECOVALEX-2019 project phase: Case 1: Fluid movement due to excavation (see section 3) and Case 2: Fluid movement due to heating (see section 4).

3 Model approaches to Case 1: Fluid movement due to excavation

Due to underground excavation of a gallery or drilling of a borehole, fluid - potentially consisting of gaseous and liquid phases - begins to move towards to the opening as observed in Paul et al. (2015). For simulating this case, the open-source finite element code OpenGeoSys (Kolditz et al., 2012) is used. As a first conceptual model strategy, a two-phase flow model coupled with a mechanical model is used to analyse different scenarios at the macroscale. The following aspects are therefore to be quantified:

- the time-dependent stress redistribution due to mechanical creep,
- the development and extent of a micro-fissure zone according to the dilatancy-criterion,
- the shortest distance *d* (Figure 4) between the domain containing the fluid inclusions and the drilled hole, which is the cause for the stress redistribution, and
- the percolation threshold for the fluid movement as a function of the capillary pressure (determined by surface tension effects between three phases) and the minimal principal stress.

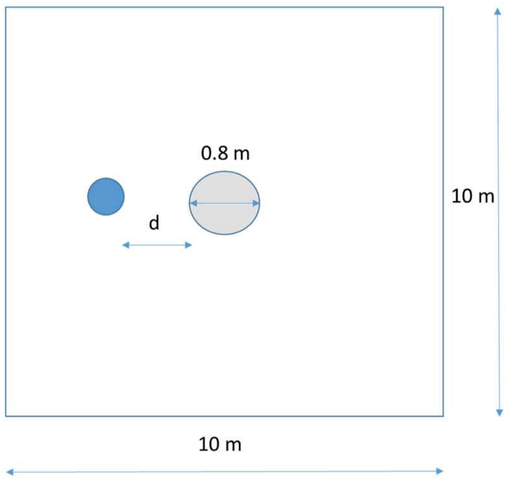

Figure 4: A two-dimensional domain with an opening (excavation) in the middle and a domain with inclusions at a distance *d* away from the opening.

3.1 Macroscale modelling of stress field after excavation

The deviatoric stress field and minimal principal stress around an underground opening play an important role in the migration of fluid inclusions. To determine the stress state, a two-dimensional model (10x10 m) is used. A hole with a diameter of 0.8 m is drilled in the middle of the domain, to introduce a disturbance to the initial stress state. The model setup for this case is shown in Figure 4. We assume that there is a fluid inclusion with a limited volume in the tight rock apart from the borehole with a distance d. This fluid inclusion is originally immobile, because

1) the system is constrained by an isotropic stress state of 25 MPa representative of a depth of about 1000 m below the ground surface,

2) the pore pressure with/without inclusion is overall equal to the stress condition and there is no hydraulic gradient, and

3) the permeability of the rock is very low.

For the macroscale modelling of the excavation process, a coupled thermomechanical model taking account of creep behaviour is used. The steady-state creep rate is calculated by using the BGRa model (Hunsche, 1993) including both elastic and steady-state deformations of the rock salt (Figure 5).

$$\dot{\boldsymbol{\varepsilon}}_{cr} = \mathrm{V} \cdot \mathrm{A} \cdot \exp\left(\frac{-\mathrm{Q}}{\mathrm{R} \cdot \mathrm{T}}\right) \cdot \left(\frac{\sigma}{\sigma^*}\right)^{\mathrm{n}}$$

Equation 1:

Where, σ is the deviatoric stress and structural factor A = 0.18 d^{-1}, activation energy Q = 54 $kJ \cdot mol^{-1}$, the universal gas constant R = $8.314 \cdot 10^{-3}$ kJ/(mol·K), stress exponent n = 5, σ^* = 1 MPa (reference value), T = Temperature in K and V=1 for rock salt with a creep class 5.

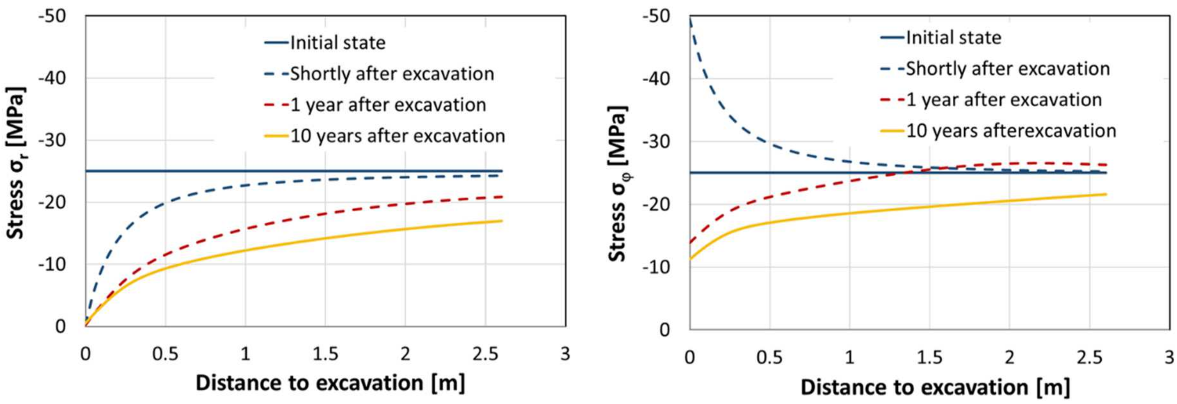

Figure 5: Time-dependent stress state in rock in the horizontal direction (radial stress σ_r and tangential stress σ_φ).

It is obvious from the simulation that the deviatoric stress state initiated by excavation changes over time due to creep (Figure 6), leading to a continuous convergence and an expansion of excavation damaged/disturbed zone (EDdZ) in the near-field of the excavation. For a dry salt rock, the (total) stress state is located within the dilatancy boundary (Figure 7). We use the well-established dilatancy criterion (Equation 2) from Hunsche et al. (1993).

$$\tau_{\mathrm{D,cr}} = 0.899 \cdot \sigma_{\mathrm{m}} - 0.0167 \cdot \sigma_{\mathrm{m}}^2$$

Equation 2

where σ_m is the mean normal stress. In case of the existence of fluid inclusions in the rock mass, a coupled hydro-mechanical model based on the effective stress concept is needed. In the applied effective stress concept using Biot's coefficient, an increase is fluid pressure indicates the reduction of effective normal stress. The stress path would move towards the criterion lines as shown in Figure 7 for all three representative points (A, B, and C) near the opening. We define a dimensionless characteristic length L/R = 0 (A), 0.6 (B) and 3.25 (C), where L is the distance between fluid location and borehole wall, and R is the radius of the borehole. These three points indicate three different zones, A = EDZ, B = EdZ and C = far-field without changed rock properties respectively. The higher the Biot's coefficient, the lower the effective normal stress. In this case, the area outside the 'original' EDZ, e.g. B and C may exceed the dilatancy limit after 10 years due to creep-induced stress redistribution (Figure 7). Therefore, micro-cracks can be generated in this area. Damage induced fractures can occur at the location of EDZ around the opening.

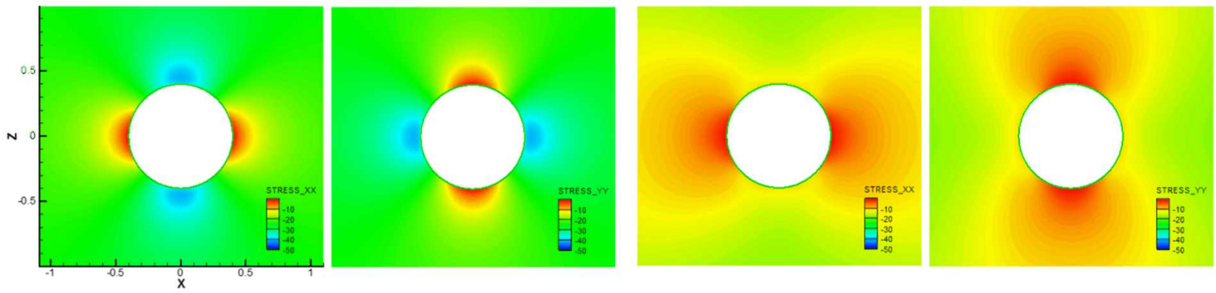

Figure 6: Simulated horizontal and vertical stress distributions immediately after the excavation (left two) and 10 years later (right two),respectively.

Table 1: Unfavourable stress conditions considered for the microscale model

	Variation - 1	Variation - 2	Variation - 3	Variation - 4	Variation - 5	Variation - 6
radius/time	L/R=0 (0.1 day)	L/R=0.6 (0.1 day)	L/R=0.6 (100 days)	L/R=3.25 (100 days)	L/R=3.25 (3000 days)	L/R=3.25 (0.1 day)
dev. stress	39.6	20	13	8.5	5.8	2.8
min. stress	0.1	15.0	8.0	19.5	13.7	23.2
max. stress	39.7	35.0	21.0	28.0	19.5	26.0

The stress state in the observation area is the mechanical conditions for a microscale analysis of fluid inclusion migration. We selected a couple of variations with large deviatoric stresses and low minimum principal stress (Table 1) as unfavourable stress conditions. The different variations were taken from different locations and times around the opening, e.g. the variation-6 is the stress state at the point C shortly after the excavation.

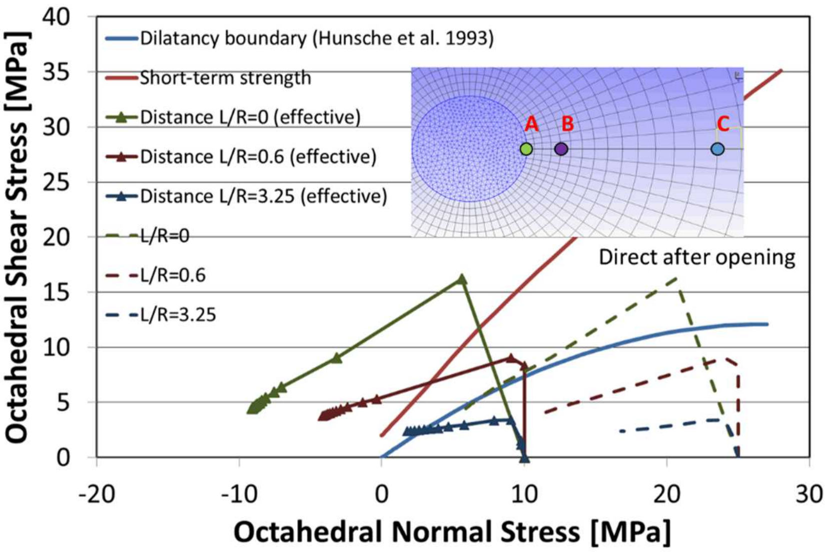

Figure 7: Stress path in the different location around an opening and the dilatancy criterion.

3.2 Microscale modelling of fluid movement based on a coupled two-phase flow and elastoplastic model

The rock salt samples show a diverse inventory of fluid inclusions preserved as bubbles, stripes, branching networks, vermicular lines and fluid films. Exemplarily, we take a CT-image of a grain boundary structure from Thiemeyer et al. (2013). In this image (Figure 8, middle) the structure of halite grain boundaries is recognisable as a network. Small volumes (black arrows) located at triple junctions of halite grain boundaries indicating the large pore space with previous fluid inclusions before sample preparation. After injection of resin, their size is somehow overrepresented.

Assume that such a structure with fluid inclusions is originally located in the near of an opening under isotropic stress conditions, e.g. at the point A, B or C. After the excavation, both hydraulic and mechanical conditions are changed. Due to the redistribution of stress around the opening, the stress state is now changed to a deviatoric stress condition as shown in Figure 8 for variation-2 (Table 1). Different models have been applied to understand the movement of such inclusions. A possible mechanism is the pathway dilatancy-controlled flow migration, which can be modelled using a coupled two-phase flow and elastoplatic model by taking into account the altered hydraulic properties of the network.

3.2.1 Finite element model for a microscale grain boundary structure

Based on the information extracted from a colour raster from a CT image, a two-dimensional high-resolution finite element mesh is generated with a maximal element length of one micrometre. Three sub-domains are used to define different materials: halite grain (blue), void space between grains (black), and partly opened pore or fracture in network filled with secondary minerals (green) (Figure 8, right). This classification of course depends on the resolution of CT techniques, where the basis for volume extraction out of CT raw data sets is given by grey value contrasts (Thiemeyer et al., 2013).

After excavation, fluid flows predominantly along the grain boundary to the tunnel (Fig. 8, left) in the defined case. Therefore, no flow boundary conditions are assumed on the upper and bottom boundaries. On the left boundary, a high hydraulic pressure (corresponding to the initial pressure) and, on the right side, a low hydraulic pressure, equal to the atmospheric pressure in the tunnel, are defined for microscale modelling (Fig. 8, middle). As initial conditions, a fully water-saturated state is assigned on open grain boundaries and a dry condition within the halite grain.

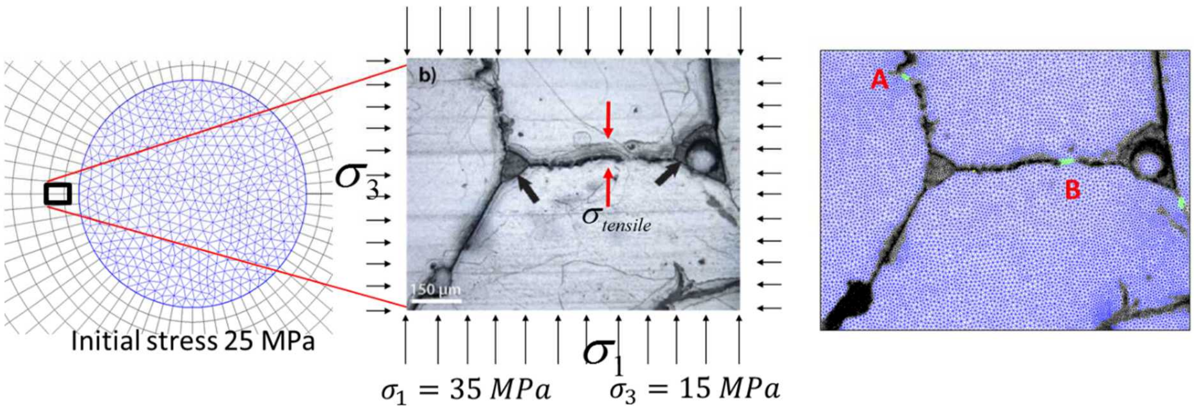

Figure 8: Stress conditions after the excavation (left) for microscale (sub-pore scale) modelling (variation 2) – CT-image of a grain boundary structure from Thiemeyer et al. (2015) (middle) and finite element mesh (right).

3.2.2 Parameter determination using rule of mixtures

Very important but also uncertain is the parameter determination of different material groups. The macroscale parameters are taken from the geotechnical synthetic analysis at the Gorleben site in Northern Germany (Bräuer et al., 2011). We assume that the halite solid has a very low permeability ($< 10^{-22}$ m²) as measured on the dry salt rock and the permeability of the network has a relative high permeability ($> 5X10^{-19}$ m²), which can be calculated using the cubic law. The permeability of the third group (partly opened pore/fracture filled with secondary minerals) can then be estimated using the rule of mixture.

We use generally the rule of mixtures, a weighted mean to calculate various properties of a composite material. From the total flux calculation in case of a flow parallel to the high permeable zone, the hydraulic conductivity of a composite system can be determined as:

$$K_x \times L_x = K_{x1} \times L_{x1} + K_{x2} \times L_{x2} + K_{x3} \times L_{x3}, \text{ where } L_x = L_{x1} + L_{x2} + L_{x3}$$

Equation 3

where K_{xi} is the permeability of the material i (i=1,2,3) and L_i is the length (2D) or surface (3D) fraction of the material i perpendicular to the flow direction as weighting functions. From the total strain calculation for an isotropic material, the mechanical Young's modulus of a composite may exhibit a lower bound (Reuss bound) (Reuss, 1929) at:

$$E=\left(\frac{f_1}{E_1}+\frac{f_2}{E_2}+\frac{f_3}{E_3}\right)^{-1}$$

Equation 4

where E_i is the E-modulus of the material i (i=1,2,3) and f_i is the volume fraction of the material i. Some values are assumed according to the general understanding, e.g. almost zero tensile strength for a grain boundary with inclusions and very low permeability of a halite solid crystal.

3.2.3 Numerical models and relationship between permeability and volumetric strain

A coupled hydro-mechanical finite element approach (two-phase flow and mechanical deformation) is used for the present study. In this model, solid displacement, gas pressure, and capillary pressure are defined as primary variables. In the simulation, an elasto-plastic model is applied, in which both shear and tensile failure with tension cut-off are considered. The relationship between capillary pressure and water saturation is described by the van Genuchten function, and the approach of Mualem is used for the relative permeability for both gas and water phase. As an important coupling factor, the intrinsic permeability is changed along with mechanical and hydraulic conditions during fluid migration.

An empirical relationship between intrinsic permeability and volumetric strain for rock salt is used (Bechtold et al., 2004):

$$k = B \cdot (\varepsilon_{\mathrm{vol}})^C$$

Equation 5

Where B and C are material parameters, which are determined in the dilatant loaded rock salt sample by laboratory experiments and $\varepsilon_{\mathrm{vol}}$ is the volumetric strain from elastic and plastic deformation (Pudewills, 2007).

It is well known that microcracks in the immediate near-field of an excavation will be generated after an underground opening. This is because the stress state there after the excavation is above the dilatancy limit (Fig. 7). The orientation of the microcracks is parallel to the tangential direction of the opening, because the radial stress decreases due to stress redistribution. Therefore, the vertically oriented grain boundary (point A in Figure 8 right) exhibits an increase in permeability as expected. In the deep area of an opening (e.g. 3.5 times the radius of the opening), no permeability change is calculated in both variation-6 and variation-4 (Table 1). The permeability of the grain boundary may increase by four to five orders of magnitude, using the empirical approach between permeability and volumetric strain (Equation 5) in the late time (10 years after the excavation) in case of variation-5 (Figure 9). At a macroscale, the permeability of the porous medium can increase up to two orders of magnitude. The time-dependent deformation on load confirms the statement that after a sufficiently long time and at already low deviatoric load, irreversible deformation may occur without damaging the material.

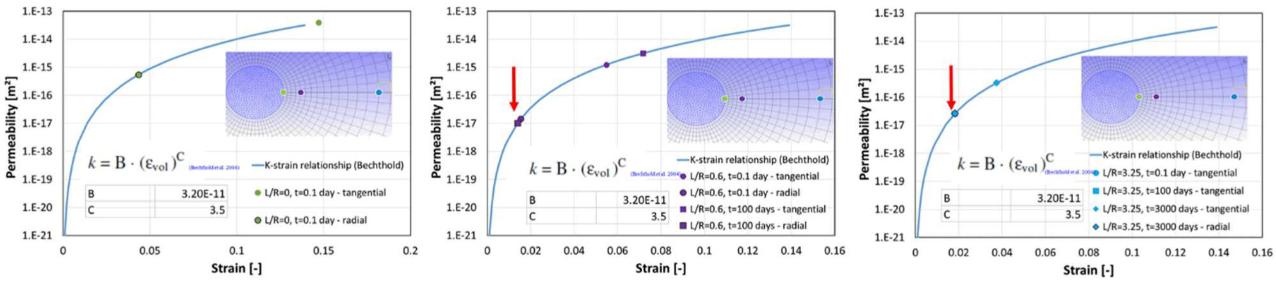

Figure 9: Permeability increase due to change of volumetric strain.

3.2.4 Pathway opening for flow under deviatoric stress condition

Even along a grain boundary, the void space may be not connected for flow to occur because of the presence of secondary minerals or halite rest. Fluid inclusions are originally separated (Figure 10, left) and in an equilibrium state. But, the relatively low tensile strength of the grain boundaries with secondary minerals in comparison with those of halite solid leads to an opening of the pathway under the high fluid pressures in conjunction with the imposed deviatoric stress state. The microscale model result demonstrates how fast (90 seconds in Figure 10) a fluid inclusion can flow through this new pathway because of the high hydraulic gradient (Figure 10, right). The calculated high velocity is a hint for the explanation of the fast pressure build-up measured in situ.

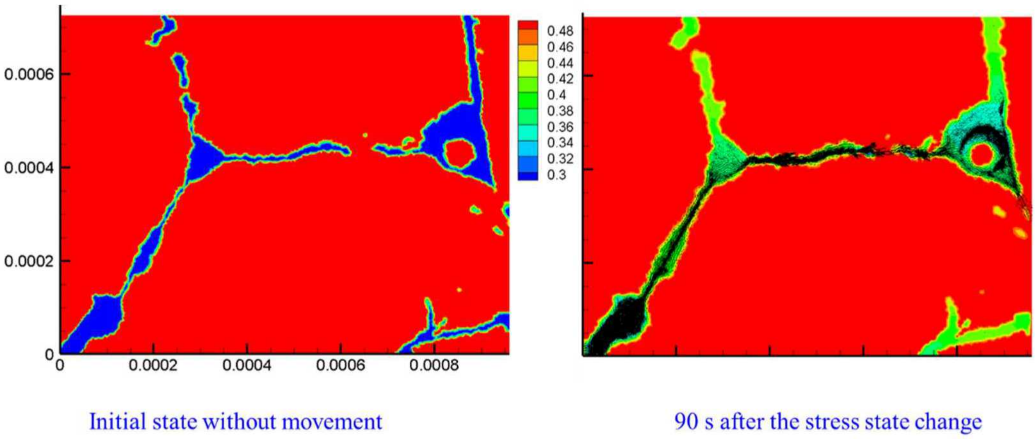

Figure 10: Migration of fluid inclusions (gas saturation) along the grain boundary in the microscale model shortly after the excavation.

4 Case 2: Fluid movement due to heating

In the post-closure phase of a repository, the stress state will evolve to the initial state due to the creep processes typically seen in rock salt if the used backfill has similar properties as the host rock (e.g. crushed salt). Due to the decay heat of waste, the salt around a waste container will be subjected to a thermal gradient. Due to the solubility difference induced by a temperature gradient, embedded fluid inclusions may move toward or away from a heating source (Figure 3) through differential dissolution/precipitation.

For this case, coupled thermal-hydro-chemical processes need to be considered:

- Mineral dissolution and precipitation within a fluid inclusion,
- Dihedral angle changes of fluid inclusions at grain boundaries,
- Thermal deformation,
- Induced porosity change, and
- Related permeability change.

4.1 Mathematical formulation

Significant progress has been made in understanding fluid inclusion migration in salt under a thermal gradient (e.g., Müller and Zschätsch 1985, Anthony and Cline 1971, Jenk 1979). A reasonable model should be able to account for the following key features of the phenomenon:

- A liquid fluid inclusion moves towards a heating source at a velocity linearly proportional to the thermal gradient imposed (Müller and Zschätsch, 1985). Interestingly, it seems that the migration velocity also depends on a mechanical loading (Jenk, 1979). Increasing the mechanical loading enhances migration.
- The velocity of inclusion migration also increases with the size of the inclusion, but not linearly (Anthony and Cline, 1971;, Jenk, 1979; Olander et al. 1982). The velocity appears to reach a plateau as the size of the inclusion increases. This plateau seems to shift to a higher value at a higher temperature. This shift becomes more pronounced for small inclusions.
- The velocity of fluid inclusion migration increases approximately exponentially with the overall temperature (Jenk, 1979).

- Complex behaviours have been observed for bi-phase inclusions. Liquid-dominated inclusions migrate upward the thermal gradient while vapour-dominated inclusions move downward the gradient. Therefore, there is a bifurcation point in a vapour/liquid ratio for the direction of inclusion movement (Anthony and Cline, 1972; Müller, 1985).
- As a fluid inclusion migrates along a thermal gradient, its shape may change, and it may break into smaller inclusions (Yagnik, 1983). Remarkably, at the advancing front of an inclusion, channelling may be developed, indicating morphological instability of the front.

To account for these features, the following dynamic model for a single fluid inclusion migration in a thermal gradient field can be formulated.

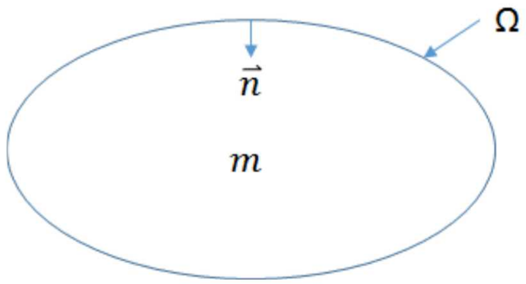

Figure 11: Modelling system for single inclusion migration in a thermal gradient field.

The model setup is shown in Figure 11. A liquid-phase fluid inclusion is enclosed in a surface Ω. We assume that the mass transfer within the inclusion can be described with a molecular diffusion process and that the thermal gradient within the inclusion is approximately identical to the ambient gradient. Within Ω, we have:

$$\frac{\partial m}{\partial t} = D(T_0)\nabla^2 m$$

Equation 6

$$\frac{\partial T}{\partial x} = \alpha$$

Equation 7

where m is the concentration of dissolved salt; D is the diffusion coefficient; T is the temperature; α is the thermal gradient; T_0 is the temperature at the centre of the inclusion; x is the coordinate along the imposed thermal gradient; and t is the time. For simplicity, we assume that the diffusion coefficient D taken at temperature T_0 can apply to the whole inclusion.

On the inner surface Ω, mineral dissolution and precipitation takes place:

$$NaCl(s) \longleftrightarrow NaCl(aq)$$

The mass balance on the surface can be described by:

$$R_d = k(K_d - m)$$

Equation 8

$$K_d(T,\kappa) = K_d^0 e^{\frac{\Delta H_r}{RT}\left(\frac{T}{T_0}-1\right)-\frac{2\gamma V_m \kappa}{RT}}$$

Equation 9

$$-D\vec{\nabla} m \cdot \vec{n} = R_d$$

Equation 10

where R_d is the mineral dissolution rate; K_d is the solubility of the mineral and k is the reaction rate constant; T_0 is the temperature at the centre of the inclusion; K_d^0 is the mineral solubility at temperature T_0; ΔH_r is the enthalpy of the mineral dissolution reaction; γ is the surface energy of the solution-salt interface; V_m is the molar volume of the salt; κ is the curvature of the surface; R is the gas constant; and $\vec{n}$ is the unit normal vector pointing inward (see Figure 12).

The evolution of the inclusion surface can be described by the following kinematic equations (Wang and Merino, 1995):

$$\Omega(x, y, z) = 0$$

Equation 11

$$\vec{\nabla}\Omega \cdot \vec{V} + \frac{\partial \Omega}{\partial t} = 0$$

Equation 12

$$\vec{V} + V_0 \vec{l} = -V_m R_d \vec{n}$$

Equation 13

$$\vec{n} = -\frac{\vec{\nabla}\Omega}{|\vec{\nabla}\Omega|}$$

Equation 14

$$\kappa = -\vec{\nabla} \cdot \vec{n}$$

Equation 15

where V_0 is the velocity of fluid inclusion migration, and $\vec{V}$ is the velocity of inclusion surface movement relative to the centre of the inclusion. Equations (6) to (15) constitute a moving boundary problem for single fluid inclusion migration along a thermal gradient. This set of equations can be solved using a level-set method.

4.2 Model analysis for inclusions with simple geometries

A first-order analysis can be conducted based on the model developed above. For a spherical liquid inclusion with a radius *r*, and assuming $k \rightarrow \infty$, the velocity of inclusion migration under a thermal gradient α can be estimated by:

$$V_0 \approx \frac{V_m D K_d^0 \Delta H_r \alpha}{R T_0^2} e^{\frac{-2\gamma V_m}{R T_0 r}}$$

Equation 16

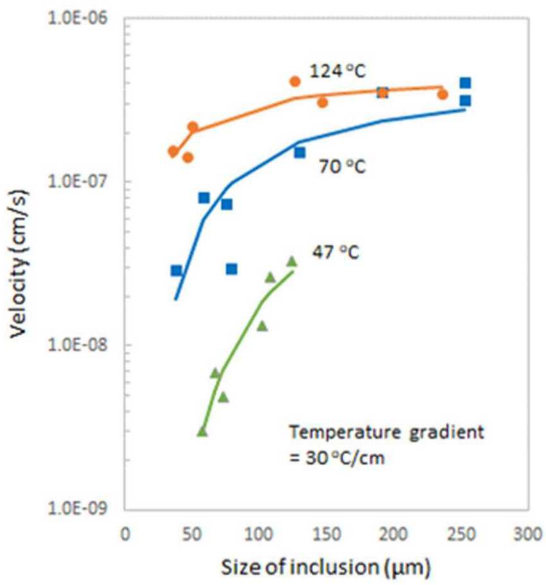

Figure 12: Fitting of equation (2-11) to the measured migration velocity as a function of inclusion size. The measurements are taken from Orlander et al. (1981). Here the size of an inclusion is taken to be the width of the inclusion originally reported in Orlander et al. (1981).

This simple equation can qualitatively explain the following key features experimentally observed:

- The model predicts a linear increase in migration velocity with increasing thermal gradient α, as observed (Müller and Zschätsch 1985).
- The model predicts that, as the size of the inclusion increases, the velocity of inclusion migration increases and then approaches a plateau (Figure 13). Also, as the temperature increases, the surface energy γ is expected to decrease (Ghanbaradeh et al., 2015), thus shifting the plateau upward. Furthermore, as the size of the inclusion decreases, the migration velocity diminishes. All these predictions are qualitatively consistent with the observations (Anthony and Cline 1971, Jenk 1979; Orlander et al. 1981). This model fitting allows us to estimate the surface tension between brine and salt for different temperatures. It is interesting to note that the values estimated for three temperatures fall on a straight line in a log (surface tension) vs. 1/T plot (Figure 14), indicating that the velocity model given in equation (16) captures the underlying physics of fluid inclusion migration in salt.
- Both terms D and K_d^0 in Equation 16 exponentially increase with temperature. At elevated temperatures, the two terms are expected to take over the term T_0^2 in the denominator in the equation, leading to an overall exponential increase in migration velocity with temperature (Jenk 1979).
- Since the solubility of a mineral depends on the stress to which the mineral is subjected (Wang, 2016), a high mechanical loading results in a higher solubility of the mineral, therefore accelerating inclusion migration (Orlander et al. 1981, Jenk 1979)).

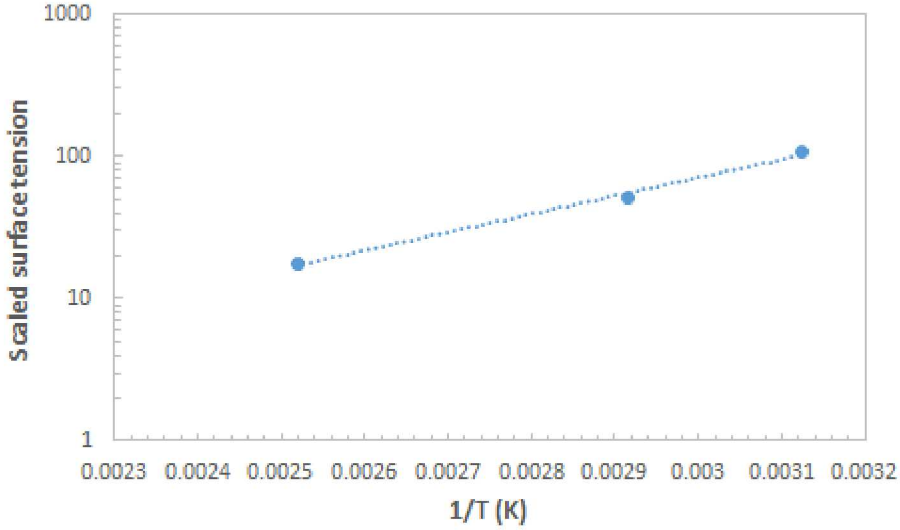

Figure 13: Scaled surface tension between brine and salt ($\frac{2\gamma V_m}{RT_0}$) estimated by fitting equation (16) to migration velocity measurements (Figure 13).

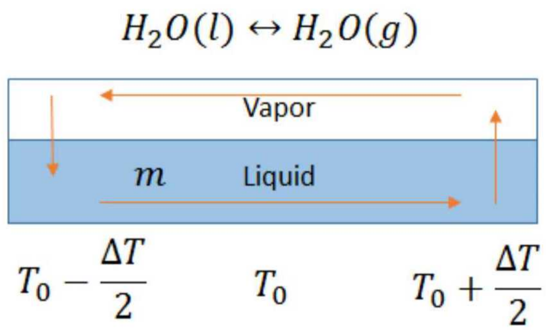

Figure 14: A simplified representation of a bi-phase fluid inclusion, in which a continuous vapour-liquid conversion takes place along a thermal gradient.

The migration of biphase vapour-liquid inclusion under a thermal gradient was studied by Anthony and Cline (1971). a simple analysis using equations (6) through (15) can also be performed for bi-phase fluid inclusions. For simplicity, a simple geometry for a fluid inclusion is assumed as shown in Fig.15. The mass continuity equations for both vapour and liquid as well as for the dissolved salt can be described by:

$$\rho_v(T) = \rho_v^0 e^{\frac{\Delta H_r^W}{RT}\left(\frac{T}{T_0}-1\right)}$$

Equation 17

$$\mathrm{A_v D_v} \frac{\partial \rho_\mathrm{v}}{\partial \mathrm{x}} = \mathrm{A_l D_l} \rho_\mathrm{w}$$

Equation 18

$$-D\frac{\partial m}{\partial x} + mV_l = 0$$

Equation 19

where ρ_v^0 is the vapour density at temperature T_0; $\rho_v(T)$ is the vapour density at temperature T; $\rho_w$is the density of the liquid; ΔH_r^W is the enthalpy of liquid-vapour phase transition; A_v and A_l are the cross section areas of vapour and liquid respectively; D_v is the diffusion coefficient of vapour;

and V_l is the local flow velocity of liquid. Assuming that the reaction rate for salt dissolution and precipitation $k \rightarrow \infty$, we obtain the bifurcation point in vapour/liquid volume ratio ($f = A_v/A_l$) for fluid inclusion migration:

$$f_c = \frac{D \Delta H_r \rho_w}{D_v \Delta H_r^w \rho_v^0(T_0)}$$

Equation 20

When $f > f_c$ the inclusion tends to move away from the heating surface, while for $f < f_c$ the inclusion tends to move upward the thermal gradient.

In the model analyses presented above, we assume that the dissolution or precipitation of salt is limited by transport. This is a reasonable assumption, based on a general observation that the dissolution of a low-solubility mineral is usually limited by surface kinetics while the dissolution of a high-solubility mineral is limited by transport (i.e., diffusion) (Berner, 1978). Our results show that the model developed based on the fast kinetics seems able to explain all the key features of experimental observations, implying that the effect of reaction kinetics on fluid inclusion migration as discussed by Anthony and Cline (1972) needs to be re-examined.

4.3 Linear stability analysis of brine-salt interface

As mentioned above, at the advancing front of an inclusion, channelling may be developed, indicating morphological instability of the front (Figure 15). The mathematical model given in equations (6) through (15) also provides a framework for studying this instability. To do so, we first apply the model to a planar interface, and then introduce an infinitively small perturbation to the interface and see if the perturbation would grow with time. Again, we assume that that the dissolution of salt is limited by diffusion. Using a standard linear stability analysis (Wang and Merino, 1995), we can show that the interface between brine and salt under a thermal gradient indeed becomes unstable, leading to fingering or channelling of the interface (a similar result was also obtained by Yagnik 1983). The wave length of the fingering is predicted to be:

$$\lambda = 2\pi \sqrt{\frac{3\beta}{\alpha\theta}}$$

Equation (21)

with

$$\theta = \frac{K_d^0 \Delta H_r}{RT_0} \quad \text{and} \quad \beta = \frac{2K_d^0 \gamma V_m}{RT_0}$$

That is, the wave length is predicted to decrease with the thermal gradient (α) and the solubility increase of salt by temperature (θ) and increase with the surface tension between brine and salt (β).

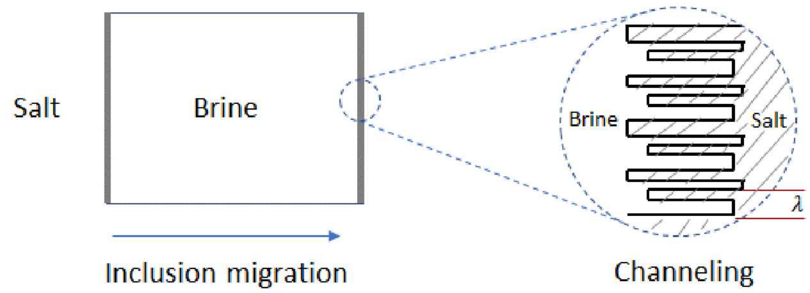

Figure 15: Morphological instability-induced channeling of a migrating brine-salt interface

Thus, different from the existing models (e.g., Anthony and Cline 1972), the model presented here in equations (6) through (15) provides a unified theoretical framework for predicting individual fluid inclusion migration and morphological evolution of a migrating brine-salt interface. The model relates fluid inclusion migration to a basic set of thermodynamic parameters (e.g., enthalpy, surface tension, etc). The simple expression for inclusion migration, equation (16), obtained from the first order approximation of the model is able to predict the key features of fluid inclusion migration observed in experiments. The result seems to indicate that the effect of interface kinetics (i.e., the finite dissolution rate of salt) may not be important as previously thought (Anthony and Cline 1972). Unlike the previous work (Anthony and Cline 1972), our work suggests that the dependence of inclusion migration velocity on inclusion size may result from the dependence of salt solubility on inclusion size (i.e., the curvature of the brine-salt interface) (Figure 12), thus eliminating a difficulty associated with the previous model (Anthony and Cline 1972, eq. 10) that predicted a unphysical negative migration velocity for small inclusions.

4.2 Numerical approaches for migrating fluid inclusions

To fully understand migration of individual fluid inclusions, the model formulated in equations (6) through (15) must be solved numerically. For thermo-mechanical (TM) and thermo-hydro-mechanical (THM) analysis of rock salt numerical approaches are available including a variety of constitutive models. We are using OpenGeoSys for TM/THM analysis in the following (e.g. Kolditz et al., 2012; Böttcher et al., 2017, Nagel et al., 2017). Strong permeability contrasts between an impermeable zone and a zone with secondary permeability due to percolation mechanisms or dilatancy-activated grain boundaries can be described by suitably defined local percolation criteria F_{perc}, e.g. related to classical dilatancy criteria, in the format

$$\text{solve:} \begin{cases} \text{(T)M} & \text{where} \quad F_{\text{perc}}(\sigma_{\text{eff}}) < 0 \\ \text{(T)HM} & \text{where} \quad F_{\text{perc}}(\sigma_{\text{eff}}) \geq 0 \end{cases}$$

Equation 21

and by enhancing the permeability tensor in a stress-dependent orthotropic manner:

$$\boldsymbol{k}(\boldsymbol{\sigma}) = \sum_{i=1}^{3} k_{(i)} \boldsymbol{n}_{(i)} \otimes \boldsymbol{n}_{(i)}$$

Equation 22

where $\boldsymbol{n}_{(i)} \otimes \boldsymbol{n}_{(i)}$ are the eigenprojections of the Cauchy stress tensor and the $k_{(i)}$ determine the permeability into the thus defined directions. The movement of fluid inclusions is conceptually different to these existing approaches. Hence, some model extensions are required for their description which will be indicated in the sequel.

Fluid inclusions migrate under the influence of temperature gradients and stress fields. The focus here is initially on single-phase liquid inclusions. The problem is addressed at two scales:

- On the microscale, fluid inclusions are resolved explicitly and their migration is governed by mechanistic laws (e.g. interface kinetics, transport in phase compartments) similar to the considerations described in Section 4.1. This requires the development of numerical methods which are able to track moving phase interfaces.

- On the macroscale, the migration of a smeared fluid phase is intended to describe the motion of fluid surrounding a disposal cell without explicitly modelling individual inclusions, as indicated in Fig. 4. Evolution/transport laws for a fluid-inclusion phase present in tight rock need to be established, informed by the microscale knowledge, and used to quantify overall fluid influx into caverns.

Both on the microscopic and the macroscopic level the analyses will base on a mixture theory/porous media theory approach. Temperature- and pressure-dependent solubilities will be at the heart of modelling the migration of fluid inclusions. For the numerical treatment of such interface problems, OpenGeoSys provides both phase-field methods (Yoshioka et al., 2019; Miao et al., 2019), locally enriched interface elements (Watanabe et al., 2012; Yoshioka et al., 2019), and analysis approaches based on configurational mechanics (Parisio et al. 2017). All the above approaches are suitable to describe interface mass transfer, surface energy and surface tension effects.

Macroscopically, an inclusion continuum will be coupled to the deforming rock salt continuum and treated numerically with the finite element method. Temperature and stress gradients may act as driving forces on the kinematics of this inclusion phase.

4.2.1 Volume and surface reactions in a porous media framework

Consider as an example the mass balance of phase α in a porous body (dissolution and precipitation are here described using *volumetric* quantities)

$$(\varrho_\alpha)'_\alpha + \varrho_\alpha \mathrm{div}\, \boldsymbol{v}_\alpha = \hat{\varrho}_\alpha \quad \text{with} \sum_\alpha \hat{\varrho}_\alpha = 0$$

Equation 23

where ϱ_α is the apparent density of phase or constituent α, $\boldsymbol{v}_\alpha$ its velocity and $(\cdot)'_\alpha$ the material time derivative following the motion of α. The density production term $\hat{\varrho}_\alpha$ can be used to describe how much salt is dissolved or precipitated at a point in space in terms of a mass rate per unit volume. Solved on a continuous domain, this allows the simulation of the motion (i.e. redistribution) of a smeared fluid-inclusion phase in a macroscopic sense. The fluid-inclusion phase velocity may be determined directly by correlating it with temperature and stress gradients, for example. As such, this macroscopic model can provide an empirically motivated model for the engineering assessment of the average motion of a distribution of fluid inclusions around an excavation or heater.

More mechanistic models may be devised on the microscale. When accounting for moving surfaces, such as on phase boundaries typical for pore-scale considerations (although macroscale phenomena can likewise be addressed), the theory needs to account for sharp phase boundaries and hence needs to be extended by jump balance equations.

Again sticking to a mass balance as an example, this jump balance reads (dissolution and precipitation are now described as *surface* reactions)

$$[\![\varrho_\alpha(\boldsymbol{v}_\alpha - \boldsymbol{v}_\Gamma)]\!] \cdot \boldsymbol{n}_\Gamma = \tilde{\varrho}_\alpha \quad \text{with} \sum_\alpha \tilde{\varrho}_\alpha = 0$$

Equation 24

where the jump brackets relate quantities on both sides (+ and -) of an interface Γ (interfacial velocity $\boldsymbol{v}_\Gamma$, $[\![\cdot]\!] = (\cdot)^+ - (\cdot)^-$. The density production term $\tilde{\varrho}_\alpha$ can be used to describe how much salt is dissolved or precipitated at a point located on the phase interface in terms of a mass rate per surface area. This allows the simulation of the motion of explicit fluid-solid interfaces and hence the evolution of inclusion position and shape.

Similar formulations can be derived for the linear momentum balance as well as the energy balance, allowing taking into account surface tension, surface energy, reaction enthalpies, etc.

Such extensions are required to capture the size/curvature-dependent behaviour observed in moving fluid inclusions (Anthony et al., 1971; Anthony et al., 1972; Roedder, 1984; Müller and Zschätsch, 1985; Müller, 1985).

For illustration, consider a simple model of salt dissolution/precipitation of a non-porous salt volume (domain -) in a brine solution (domain +) can be realized by allowing for α = {**s**olid salt, **w**ater, sol**u**te (dissolved salt)} with

$$
\begin{aligned}
\tilde{\varrho}_\mathrm{s} &= -\tilde{\varrho}_\mathrm{u} = h\big[\tilde{\varrho}_\mathrm{u}^{+} - \tilde{\varrho}_\mathrm{u}^{\mathrm{eq}}(T, \mathrm{tr}\,\boldsymbol{\sigma}^{-}|_{\Gamma}, \dots)\big] \quad \text{with } \tilde{\varrho}_\mathrm{w} = 0 \\
\varrho_\mathrm{s}^{-} &= \varrho_\mathrm{sR} \\
\varrho_\mathrm{s}^{+} &= \varrho_\mathrm{w}^{-} = \varrho_\mathrm{u}^{-} = 0
\end{aligned}
$$

Equation 25

Note that in the case of a dissolving porous material this porous domain would also contain solvent and solute, i.e. $\varrho_\mathrm{w}^{-}, \varrho_\mathrm{u}^{-} \neq 0$. In that case, volumetric dissolution may additionally be considered by postulating a similar relationship for $\hat{\varrho}_\mathrm{s}$ as done here for $\tilde{\varrho}_\mathrm{s}$. The above model indicates that pressure- and temperature-dependent solubilities are considered via $\tilde{\varrho}_\mathrm{u}^{\mathrm{eq}}(T, \mathrm{tr}\,\boldsymbol{\sigma}^{-}|_{\Gamma}, \dots)$. With the assumption of either well-stirred baths, diffusive mass transport or explicit process calculations, the above model can be used to solve for the interface velocity $\boldsymbol{v}_\Gamma$, see Section 4.1 as well as Ateshian 2011 for more details on such an approach.

4.2.2 Numerical methods

In Section 4.1, an approach requiring interface tracking in a numerical environment has been presented. In Section 3, grain boundary interfaces were meshed with volumetric elements making it difficult to include anisotropic deformation-dependent permeability (i.e. preferential flow along an interface where the permeability depends on a widening of the interface). In order to provide avenues for future improvements for these two approaches, possible methods for these evolving interface problems available in OpenGeoSys will be briefly described (Lu et al., 2017; Lu et al., 2018).

Typically, methods suitable for representing discontinuities/pore-scale phenomena include front-tracking methods, lattice element methods, volume-of-fluid methods, phase-field methods, level-set methods, smoothed particle hydrodynamics, remeshing techniques (r-adaptivity), and others.

On the microscale, dissolution/precipitation has been modelled by phase-field approaches (Xu and Meakin, 2008; Xu and Meakin, 2011), level-set methods (Xu et al., 2012) using finite difference schemes, or smoothed particle hydrodynamics (Tartakovsky et al., 2007), among others. Li et al. (2010) studied void migration and growth in irradiated materials using phase-field methods, explicit time integration and Fourier transforms. A multiscale finite element model has been used to study damage evolution in deformed continua by void growth driven by configurational forces on the void's surfaces in (Timmel et al., 2009).

Our approach rests on two numerical approaches: phase-field methods and locally enriched finite element approximations. For brevity, we will here only describe the former approach applicable to the problem type discussed in Section 4.1. The locally enriched lower-dimensional interface formulation, on the other hand, is suitable for describing the grain boundary flow processes with deformation-dependent permeability as discussed in Section 3. We refer the reader to Watanabe et al. (2012) and Yoshioka et al. (2019) for details on the fully coupled hydro-mechanical implementation used. Both numerical formulations rest on an implicit finite element scheme.

Phase-field methods are generally based on an order parameter *d* and can be theoretically founded on a free energy functional formulated as

$$\Psi = \int_{\Omega} \psi(d, \mathrm{grad}\ d)\mathrm{d}\Omega \quad \text{with} \quad \psi = \psi_{\mathrm{bulk}}(d) + \psi_{\mathrm{surf}}(\mathrm{grad}\ d)$$

Equation 26

where the free energy density is often additively decomposed into bulk as well as interfacial energy contributions, $\psi_{\mathrm{bulk}}(d)$ and $\psi_{\mathrm{surf}}(\mathrm{grad}\ d)$, respectively.

Most commonly, the Ansatz $\psi_{\mathrm{surf}}(\mathrm{grad}\ d) = \frac{\epsilon}{2}|\mathrm{grad}\ d|^2$ is chosen, where ϵ is a regularisation parameter characterizing the width of the phase transition zone providing the process with an internal length scale. This approach can give rise to both standard and extended Cahn-Hilliard and Allen-Cahn (Ginzburg-Landau) equations. Especially in the case of extended theories, a connection to configurational mechanics can be established (Gurtin, 1996;, Miao et al., 2019).

In a series of papers on isothermal dissolution/precipitation (Xu and Meakin, 2008; Xu and Meakin, 2011), Xu and co-workers implemented the following equations into an explicit finite difference scheme:

$$\tau \frac{\partial d}{\partial t} = \epsilon^2 \mathrm{div\ grad}\ d + (1 - d^2)(d - \lambda c) - \epsilon^2 \kappa |\mathrm{grad}\ d|$$

$$\frac{\partial c}{\partial t} = D\ \mathrm{div\ grad}\ c + \alpha \frac{\partial d}{\partial t}\left(1 + \frac{D\ \mathrm{div\ grad}\ d - \frac{\partial d}{\partial t}}{k\ |\mathrm{grad}\ d|}\right)$$

$$\tau = \alpha\lambda \frac{\epsilon^2}{D}\left(\frac{5}{3} + \frac{\sqrt{2}D}{k\epsilon}\right)$$

Equation 27

The coupling terms between phase field *d* and concentration field *c* were derived based on sharp-interface asymptotic analysis (Xu and Meakin, 2008). This model needs to be extended to non-isothermal conditions for the problem class addressed herein by including an energy balance to obtain the temperature field (or by prescribing an external pressure gradient as done in Section 4.1) and temperature-dependent solubilities $\tilde{\varrho}_{\mathrm{u}}^{\mathrm{eq}}(T)$ as alluded to above. The integration of the microstructural models described in the previous sections into these numerical frameworks is ongoing work.

5 Conclusions

Fluid inclusions are found within mineral crystals or along grain boundaries in bedded and domed salt rocks and can migrate in the presence of thermal and hydro-mechanical gradients, as supported by numerous laboratory experiments and field observations. Recent observations with microscopic techniques, e.g. computed tomography scans (CT) or scanning electron microscopy (SEM), provide additional microscale information about the morphology and structure of the composition of such inclusions. Measurements of pressure build-up and outflow from boreholes during underground excavation confirm rapid transport of such inclusions if the initial mechanical, thermal and/or hydraulic states are changed.

Fluid inclusions may migrate against the thermal gradient resulting from heat emitting radioactive waste canisters in a rock salt. Small inclusions from some distance around may migrate towards waste canisters and fluids concentrate there. This fluid transport mechanism can lead to the influx of water into storage cavities and, therefore, affect canister corrosion processes. Likewise, the migration of some inclusions away from the heat source can constitute an additional radionuclide transport mechanism. Process understanding and quantitative estimation of related migration rates and total volumes of fluid are therefore important for the repository design. The present paper compiles existing experimental investigations and - based on this - suggests specific modelling approaches for micro- and macroscale analyses of fluid inclusion migration:

- On the microscale, fluid inclusions are resolved explicitly and their migration is governed by mechanistic laws (e.g. interface kinetics, transport in phase compartments, etc.). This requires the development of numerical methods, which are capable of tracking moving phase interfaces.
- On the macroscale, the migration of a smeared fluid phase is intended to describe the motion of fluid surrounding a disposal cell without explicitly modelling individual inclusions, i.e. in a form suitable for safety assessment. Evolution laws for a fluid-inclusion phase present in tight rock need to be established, informed by the microscale knowledge where appropriate, and used to quantify overall fluid influx into caverns.

The hydro-mechanical boundary conditions for the microscale analysis are taken from the macroscale modelling. The model parameters for the microscale modelling are determined with the help of the rule of mixtures on the basis of laboratory and field measurement results from macroscale. The determining factors for the migration of fluid inclusions include changing stress conditions, hydraulic gradients after excavation, high initial fluid pressure, and the change of material properties. As a result, the permeability of the grain boundary will increase about four to five orders of magnitude according to the empirical permeability-strain model, and possible flow paths will consequently be generated – which was proofed by a numerical experiment (cf. Fig. 10). Therefore, due to the time-dependent deviatoric stress state and the ongoing stress redistribution around the cavity due to the creep behaviour of salt, fluid inclusions with high pressure originally outside of an EDZ (excavation damage zone) may begin to move quickly after a longer period of an open cavity. The model result demonstrates that a fluid inclusion can flow through this new pathway within several seconds as observed in the field measurement.

The hypothesis is quite strong and its adequacy should be assessed in more detail in the future. Sensitivity analysis will help to quantify the uncertainty of parameters used in the microscale modelling. However, the estimated permeability increase in the different zones around an opening makes the statement true that individual locally isolated inclusions between grain boundaries can flow out at high velocity under unfavourable hydraulic and mechanical conditions, as it was observed in some boreholes with intensive pressure build-up in the underground facility. Fluid inclusions are important transport mechanisms in tight geological formations, and an integrated experimental and numerical investigation using novel simulation approaches is needed.

Acknowledgements

DECOVALEX is an international research project comprising participants from industry, government and academia, focusing on development of understanding, models and codes in complex coupled problems in sub-surface geological and engineering applications. DECOVALEX-2019 is the current phase of the project. The authors appreciate and thank the DECOVALEX-2019 Funding Organisations Andra, BGR, CNSC, US DOE, ENSI, JAEA, IRSN, KAERI, NWMO, RWM, SÚRAO, SSM and Taipower for their financial and technical support of the work described in this paper. The statements made in the paper are, however, solely those of the authors and do not necessarily reflect those of the Funding Organisations.

The work of BGR was supported by BMWi (Bundesministerium für Wirtschaft und Technologie, Berlin). UFZ's work is supported by the iCross-Project „Integrity of Nuclear Waste Repository Systems" which is funded by the Helmholtz Association (grant ID SO-093) and BMBF (Bundesministerium für Bildung und Forschung) as well as the GeomInt-Project "Geomechanical integrity of host and barrier rocks - experiment, modeling, and analysis of discontinuities" (grant ID 03G0866A) funded by BMBF. Sandia National Laboratories is a multi-mission laboratory managed and operated by National Technology and Engineering Solutions of Sandia, LLC., a wholly owned subsidiary of Honeywell International, Inc., for the U.S. Department of Energy's National Nuclear Security Administration under contract DE-NA-0003525. The work performed at Sandia was supported by DOE Spent Fuel Waste Science & Technology (SFWST) Program.

REFERENCES

Al-Gharbi, M.S., 2004. Dynamic Pore-Scale Modelling of Two-Phase Flow, Dissertation, Imperial College London.

Anthony, T. R., Cline, H. E., 1971. Thermal migration of liquid droplets through solids, J. Applied Physics, 42, 3380-3387.

Anthony, T. R., Cline, H. E., 1972. The thermomigration of biphase vapor-liquid droplets in solids, Acta Metallurgica, 20, 247-255.

Ateshian, Gerard A, 2011. The role of mass balance equations in growth mechanics illustrated in surface and volume dissolutions. In: Journal of Biomechanical Engineering 133.1, p. 011010.

Bechthold, W., Smailos, E., Heusermann, S., Bollingerfehr, W., Bazargan S.B., Rothfuchs, T., Kamlot, P., Grupa, J., Olivella, S., Hanse, F.D., 2004. Backfilling and sealing of underground repositories for radioactive waste in salt, final report, EUR-20621-EN.

Berner, R. A. (1978) Rate control of mineral dissolution under earth surface conditions, Am. J. Sci., 278, 12345-1252.

Birkholzer, J.T., Bond, A.E., Hudson, J.A., Jing, L., Tsang, C.-F., Shao, H., Kolditz, O., (2018): DECOVALEX-2015: an international collaboration for advancing the understanding and modeling of coupled thermo-hydro-mechanical-chemical (THMC) processes in geological systems. Environ. Earth Sci. 77 (14), art. 539

Blunt, M. J., 2001. Flow in porous media – pore-network models and multiphase flow, current opinion in colloid and interface science 6(2001), 197-207, Elsevier.

Böttcher, N., Görke, U.-J., Kolditz, O., Nagel, Th., 2017. Thermomechanical investigation of salt caverns for short-term hydrogen storage. In: Environmental Earth Sciences 76.3, p. 98. ISSN: 1866-6280.

Bräuer, V., Eickemeier, R., Eisenburger, D., Grissemann, C., Hesser, J., Heusermann, S., Kaiser, D., Nipp, H.-K., Nowak, T., Plischke, I., Schnier, H., Schulze, O., Sönnke, J., Weber, J.-R., 2011. Description of the Gorleben site Part 4: Geotechnical exploration of the Gorleben salt dome. Bundesanstalt für Geowissenschaften und Rohstoffe, Hannover, ISBN: 978-3-510-95988-4.

Catalano, E., Chareyre, B., Cortis, A., Barthelemy E., 2011. A Pore-scale hydro-mechanical coupled model for geomaterials, II International Conference on Particle-based Methods - Fundamentals and Applications, PARTICLES 2011.

Ferrari, A., 2014. Pore-scale modeling of two-phase flow instabilities in porous media, Dissertation, University of Torino (Italy).

Ghanbarzadeh, S., Hesse, M. A., Prodanović, M., Gardner, J. E., 2015. Deformation-assisted fluid percolation in rock salt, Science, 250, 1069-1072.

Glowinski, R., Pan, T.W., Hesla, T.I., Joseph, D.D., Periaux, A., 2001. Fictious Domain Approach to the Direct Numerical Simulation of Incompressible Viscous Flow past Moving Rigid Bodies: Application to Particulate Flow. Journal of Computational Physics 2:(169)363-426.

Gurtin, Morton E., 1996. Generalized Ginzburg-Landau and Cahn-Hilliard equations based on a microforce balance. In: Physica D: Nonlinear Phenomena 92.3, pp. 178–192.

Hammer, J., Pusch, M., Häger, A., Scheeder, G., Shao, H., Paul, B., Ostertag-Henning, Ch., Mingerzahn, G., Schlömer, St., Hesser, J., 2013. Untersuchungen von Kohlenwasserstoffen im Erkundungsbergwerk Gorleben, BGR-Report, 2013.

Han, K., Feng, Y.T., Owen, D.R.J., 2007. Coupled Lattice-Boltzmann and discrete element modelling of fluid-particle interaction problems. Computer and Structures 85:1080-1088.

Hunsche, U., 1993. Strength of rock salt at low mean stress, Geotechnik-Sonderheft, Glückauf, Essen, pp. 160-163, 1993.

Jenks, G. H., 1979. Effects of Temperature, Temperature Gradients, Stress, and Irradiation on Migration of Brine Inclusions in a Salt Repository, Oak Ridge National Laboratory, ORNL-5526.

Knauth, M., Minkley, W., 2018. Back analysis of pressure driven percolation at the Weeks Island Mine. In: Proceedings of the mechanical behaviour of Salt IX, Hannover, Sept. 12-14, 2018, ISBN: 978-3-9814108-6-0.

Kolditz, O., Shao, H., Görke, U.-J., Wang, W., 2012. Thermo-hydro-mechanical-chemical processes in fractured porous media. Benchmarks and examples. Vol. 86. Lecture Notes in Computational Science and Engineering. Springer. ISBN: 9783642271779.

Leben, R.A., Dawson, P.R., Kern, H. M., Wenk, H.R., 2003. Heterogeneous deformation and texture development in halite polycrystals: Comparison of different modeling approaches and experimental data, Tectonophysics, 370 (2003) 287-311, Elsevier Publisher.

Lu, R., Watanabe, N., He, W., Jang, E., Shao, H., Kolditz, O., Shao, H., 2017. Calibration of water–granite interaction with pressure solution in a flow-through fracture under confining pressure, Environmental Earth Sciences 76.12, p. 417. ISSN: 1866-6280.

Lu, R., Nagel, T., Shao, H.B., Kolditz, O., Shao, H., 2018. Modeling of Dissolution-Induced Permeability Evolution of a Granite Fracture Under Crustal Conditions, Journal of Geophysical Research: Solid Earth, 123 (7), 5609 - 5627. ISSN: 21699313.

Miao, X.-Y., Kolditz, O., Nagel, T., (2019): Modelling thermal performance degradation of high and low-temperature solid thermal energy storage due to cracking processes using a phase-field approach. Energy Conv. Manag. 180 , 977 - 989Minkley, W., Brückner, D., Lüdeling, C., 2018. Percolation in salt rocks. In: Proceedings of the mechanical behaviour of Salt IX, Hannover, Sept. 12-14, 2018, ISBN: 978-3-9814108-6-0.

Müller, E., Zschätsch, B., 1985. Migration of brine inclusions through grain boundaries in rock salt, In: Crystal Research and Technology 20.1, K1–K3.

Müller, E., 1985. The migration of gas-filled brine inclusions in rock salt under a temperature gradient. In: Crystal Research and Technology 20.4, pp. 521–526. ISSN: 1521-4079.

Nagel, T., Minkley, W., Böttcher, B., Naumov, D., Görke, U.-J., Kolditz, O., 2017. Implicit numerical integration and consistent linearization of inelastic constitutive models of rock salt. In: Computers & Structures 182, pp. 87–103. ISSN: 00457949.

Öiu, Y., Gilormini, P., Castaneda, P. P., 2005. Homogenization estimates for texture evolution in halite, Technonophysics, Elsevier doi:10.1016/j.tecto.2005.06.007.

Olander, D. R., Machiels, A. J., Balooch, M., Yagnik, S. K., 1982. Thermal gradient migration of brine inclusions in synthetic alkali halide single crystals, J. Applied Physics, 53, 669-681.

Parisio, F., Naumov, D., Kolditz, O., Nagel, T., 2017. Material forces: An insight into configurational mechanics. Mech. Res. Commun. 93, 114 – 118.

Paul, B., Shao, H., Hesser, J., Ostertag-Henning, Ch., Lege, Ch., 2015. In-Situ Quantification of Hydrocarbon in an Underground Facility in Tight Salt Rock, Engineering Geology for Society and Territory – Vol. 6, PP 893 – 896, Springer, 2015.

Pinyol, N., Alonso, E., Gens, A., 2012. Modelling Compacted Soil Behaviour Including Microstrutural Features, Unsaturated soils Research and Applications, Vol. 2 Springer.

Pudewills, A., 2007. Modellierung des mechanischen Verhaltens von Steinsalz: Vergleich aktueller Stoffgesetzte und Vorgehensweisen, Forschungszentrum Karlsruhe FZKA7313.

Reuss, A., 1929. Berechnung der Fließgrenze von Mischkristallen auf Grund der Plastizitätsbedingung für Einkristalle. Zeitschrift für Angewandte Mathematik und Mechanik. 9: 49–58. doi:10.1002/zamm.19290090104.

Roedder, E., 1970. Application of an improved crushing microscope stage to studies of the gases in fluid inclusions. Schweizerische Mineralogische und Petrographische Mitteilungen, 50, 41-58.

Roedder, E., 1984. The fluids in salt, American Mineralogist, 69, 413-439.

Schenk, O., Urai, J.L., 2004. Microstructural evolution and grain boundary structure during static recrystallization in synthetic polycrystals of sodium chloride containing saturated brine. In: Contributions to Mineralogy and Petrology, 146(6) 2004, 671-682 - Springer.

Schlich, M., 1986. Simulation der Bewegung von im Natürlichen Steinsalt enthaltener Feuchte im Temperaturfeld – ein Beitrag zur Problematik der Endlagerung hochradioaktiver Abfälle, Bericht EUR 10672DE, Kommission der Europäischen Gemeinschaften.

Tartakovsky, Alexandre M., Meakin, P., Scheibe, T.D., Rogene M Eichler West, R.E., 2007. Simulations of reactive transport and precipitation with smoothed particle hydrodynamics. In: Journal of Computational Physics 222.2, pp. 654–672.

Thiemeyer, N., Pusch, M., Hammer, J., Zulauf, G., 2013. Quantification and 3D visualisation pf pore space in Gorleben rock salt: Constraints from CT imaging and microfabrics, Z. Dt. Gers. Geowiss, Dec. 2013.

Thiemeyer, N., Habersetzer, J., Peinl, M., Zulauf, G., Hammer, J., 2015. The application of high resolution X-ray computed tomography on naturally deformed rock salt: Multi-scale investigations of the structural inventory, Journal of Structural Geology, 77, 2015 PP92-106, 2015.

Timmel, M., Kaliske, M., Kolling, S., 2009. Modelling of microstructural void evolution with configurational forces. In: ZAMM-Journal of Applied Mathematics and Mechanics/Zeitschrift für Angewandte Mathematik und Mechanik 89.8, pp. 698–708.

Urai, J.L., Spiers, C.J., Peach, C.J., Franssen, R.C.M.W., Liezenberg, J.L., 1987. Deformation mechanisms operating in naturally deformed halite rocks as deduced from microstructural investigations. – Geol. Mijnbouw, 66: 165–176.

Urai, J.L., Spiers, C.J., 2007. The effect of grain boundary water on deformation mechanisms and rheology of rocksalt during long-term deformation. In the Mechanical behavior of Salt – Understanding of THMC Processes in Salt: 6th Conference (SaltMech 6), Hannover, 2007, ISBN: 9780415443982.

Xu, W.J., Shao, H., Hesser, J., Wang, W., Schuster, K., Kolditz, O., 2013. Coupled multiphase flow and elasto-plastic modelling of in-situ gas injection experiments in saturated claystone (Mont Terri Rock Laboratory), Engineering geology, 157: 55-68, Elsevier.

Xu, Z.J., Meakin, P., 2008. Phase-field modeling of solute precipitation and dissolution. In: The Journal of chemical physics 129.1, p. 014705.

Xu, Z.J., Meakin, P., 2011. Phase-field modeling of two-dimensional solute recipitation/dissolution: Solid fingers and diffusion-limited precipitation. In: The Journal of chemical physics 134.4, p. 044137.

Xu, Z.J., Huang, H., Li, X., Meakin, P., 2012. Phase field and level set methods for modeling solute precipitation and/or dissolution. In: Computer Physics Communications 183.1, pp. 15–19.

Wang, Y., 2016: On subsurface fracture opening and closure, J. Petroleum Sci. Eng., 155, 46-53.

Wang, Y., Merino, E., 1995. Origin of fibrosity and banding in agates from flood basalts, Am. J. Sci., 295, 49-77.

Watanabe, N., Wang, W., Taron, J., Görke, U.J., Kolditz, O., 2012. Lower-dimensional interface elements with local enrichment: application to coupled hydro-mechanical problems in discretely fractured porous media. Int. J. Numer. Methods Eng. 90 (8), 1010 – 1034.

Yagnik, S. K., 1983. Interfacial stability of migration brine inclusions in alkali halide single crystals supporting a temperature gradient, J. Crystal Growth, 62, 612-626.

Yoshioka, K., Parisio, F., Naumov, D., Lu, R., Kolditz, O., Nagel, T., 2019. Comparative verification of discrete and smeared numerical approaches for the simulation of hydraulic fracturing. GEM - Int. J. Geomath. 10 (1), art. 13.